



HAL
open science

Small-scale single burning item test for the study of the fire behavior of building materials

Alexandre Gossiaux, Pierre Bachelet, Séverine Bellayer, Stefan Ortgies, Alexander König, Sophie Duquesne

► To cite this version:

Alexandre Gossiaux, Pierre Bachelet, Séverine Bellayer, Stefan Ortgies, Alexander König, et al.. Small-scale single burning item test for the study of the fire behavior of building materials. *Fire Safety Journal*, 2021, *Fire Safety Journal*, 125, pp.103429. 10.1016/j.firesaf.2021.103429 . hal-03612707

HAL Id: hal-03612707

<https://hal.univ-lille.fr/hal-03612707>

Submitted on 22 Aug 2023

HAL is a multi-disciplinary open access archive for the deposit and dissemination of scientific research documents, whether they are published or not. The documents may come from teaching and research institutions in France or abroad, or from public or private research centers.

L'archive ouverte pluridisciplinaire **HAL**, est destinée au dépôt et à la diffusion de documents scientifiques de niveau recherche, publiés ou non, émanant des établissements d'enseignement et de recherche français ou étrangers, des laboratoires publics ou privés.



Distributed under a Creative Commons Attribution - NonCommercial 4.0 International License

Small-scale single burning item test for the study of the fire behavior of building materials

Alexandre GOSSIAUX^a, Pierre BACHELET^a, Séverine BELLAYER^a, Stefan ORTGIES^b, Alexander KÖNIG^c and Sophie DUQUESNE^a

^aUniv. Lille, CNRS, INRAE, Centrale Lille, UMR 8207 - UMET - Unité Matériaux et Transformations, F-59000 Lille, France

^bBASF Polyurethanes GmbH, Elastogranstraße 60, 49448 Lemförde, Germany

^cBASF SE, Carl-Bosch-Str. 58, 67056 Ludwigshafen am Rhein, Germany

Abstract

A small-scale single burning item test has been developed to allow quicker, easier and less costly development studies of building materials presenting high performance. The test is fully described including the dimensions of the equipment, the procedure used to perform the test, but also the methodology used for the calibration of the heat release rate (HRR) and smoke production. To study the efficiency of the test, different rigid polyurethane and rigid polyisocyanurate foams, with and without flame retardants, are used as case studies and their fire behavior evaluated. The small-scale single burning item test allowed discriminating the different foams in terms of HRR and flame spread, but also in terms of FIGRA and SMOGRA index. It also permits an easy use of additional sensors (thermocouples) leading to a better understanding of the fire behavior. The results were compared to data obtained from the mass loss cone (ISO13927). The results in terms of HRR and smoke lead to similar conclusion but compared to mass loss cone, the small-scale single burning item test makes it possible to access the flame spread behavior of the materials, which is a crucial parameter and leads to an additional discrimination of the performance of the materials.

Keywords Fire testing, polyurethane foam, polyisocyanurate foam, flame retardant, single burning item

1. Introduction

A common awareness of environmental factors and more particularly of global warming makes it urgent to better control energy consumption and reduce pollutant emissions. One solution is to reduce energy loss in building using new and efficient thermal insulation materials such as polymeric foams. When a house is heated, the exchange of temperatures with the outside causes energy losses. These losses are estimated to vary from 16 % to 25 % through the walls, 13 % to 15 % through the windows and up to 30 % through the roof. Thus, an efficient insulation allows to reduce the energy consumed to keep the house cold in summer or to heat the house in winter. Therefore, the use of natural resources (oil and gas reserves) to keep the temperature constant in the building will be reduced [1]. Thus, it is therefore in the general interest to promote the use of new insulation materials in order to reduce greenhouse gas emissions. On the other hand, organic thermal insulation materials are extremely flammable materials. Thus, the use of fireproof synthetic materials has become not only a scientific issue, but also an economic and social need in order to avoid dramatic event of fire [2,3]. Therefore, the importance of having high-performance and fire-resistant insulative materials is crucial.

Organic polymers such as polyurethane foams have a high carbon and hydrogen content that makes them highly vulnerable to fire. Flame retardants (FRs) are used in their formulation to prevent the outbreak of a fire. These additives could modify the rate of decomposition of polymers, decrease the intensity of combustion, reduce the amount of released combustible gases and also increase the ignition time [4]. Nowadays, fires casualties or damages are decreasing thanks to technological and scientific developments that make it possible to improve manufactured products in order to make them as fire resistant as possible. However, even if FR materials are used, the unfolding of a fire and its spread sometimes remain chaotic and random due to uncontrolled environmental constraints [5]. Therefore, in order to improve the understanding of the fire behavior of materials, many fire tests have appeared. In addition, many standards have also emerged in order to implement stricter regulations on the use of materials.

Fire tests provide information on the evolution of combustion and decomposition of the material in a certain range of defined environment [6]. However, even if large-scale or intermediate-scale fire tests allow to obtain reliable information close to real fire conditions, the cost of this implementation remains high. They appear as a hindrance to the development of new materials and, therefore, are generally only performed for classification purpose.

In the field of building materials, each country in Europe had stated regulations regarding their own idea of risk. Some consider the rate of heat release as the most important parameter while others consider the flame spread or smoke as equally important [7]. Because of the singularity of the systems, test rankings have emerged and a harmonization of standards was carried out in Europe in order to be based on a single classification for certain types of material. This new harmonized classification is called in Europe: Euroclasses. Among this new classification, a test has been established: the Single Burning Item test (SBI) (EN13823) [8]. The SBI test simulates a scenario of combustion of an isolated object in a corner of a room. The flame is produced by burning propane spread through a sand bed to produce a burner output of 30.7 ± 2 kW. The corner fire test causes more drastic conditions than a free fire. Indeed, the corner reduces air entrainment into the fire plume, increasing the mean and peak flame heights. Moreover, the flame height fluctuation in confined fire is larger than that of free fires. Finally, the corner made by the two panels increases the thermal radiation between them [9–11]. SBI test allows the acquisition of several types of data such as FIGRA (fire growth rate) and SMOGRA (smoke development rate). This test requires the use of two panels of 1.50 m x 1 m and 1.50 m x 0.5 m respectively and is, as previously noted, exclusively dedicated to classification.

In this context, the development of scaled-down tests to allow a more efficient way to develop materials is important. This approach was previously followed in 2013 by Bourbigot *et al.* who have developed a reduced scale (1/8) test bench based on the Steiner tunnel (Fire test from USA standard) [12]. In 2015, Tranchard *et al.* have created a test complying with two certifications in the field of aeronautics and allowing the study of the condensed phase and gas phase simultaneously during the decomposition of a material [13]. Regarding the SBI test, the approach of De Corso *et al.* is the only one reported in the literature. In that study, they have developed a mini SBI test at lab scale using the structure of the cone calorimeter as support to burn their samples [14]. De Corso *et al.* used a gas burner delivering a power between 2 kW and 5 kW. However, the use of the cone calorimeter limits, on the one hand, the size of the samples used which limits the lateral propagation of the flame on the surface and on the other hand, it does not allow a routine and exclusive dedicated use. Finally, a mini-SBI has been developed by a Danish company called "DBI fire

and security", with aim was to predict quickly and at low cost, the fire behavior of materials. However, this test has not been published in literature.

In order to avoid the creation of test bench mimicking the SBI operation, prediction models have also been proposed. Hakkarainen *et al.* [15] and Van Hees *et al.* [16] developed in 2001 and 2002 respectively models using cone calorimeter results for certain materials to predict their heat release rate curve that could be obtained using the SBI test.

Since no publication reports the development of a M-SBI test, the objective of this study is to highlight the development of a small-scale Single Burning Item test (M-SBI) with a main goal: the M-SBI test has to be used for research and development and not for product compliance. The first objective is to reduce the cost of the development by reducing the sample size. Smaller samples could generally be prepared at lab scale that is not the case for large scale SBI test that usually need semi-industrial trials. Moreover, the development of a reduced-sized test makes it easier to add different kinds of sensors giving valuable information regarding the mode of combustion of materials and the mode of action of FRs when used. For instance, thermocouples can be added into the foam and camera can be used to monitor the lateral propagation of the flame. Therefore, it will also be possible to better understand the fire behavior of foams in a fire scenario that is closer to SBI test than when lab-scale tests such as the cone calorimeter (ISO5660) or the mass loss calorimeter (ISO13927) are used. In order to achieve all these objectives, the size of the samples and of the burner were reduced by three. This down scaling is the result of a compromise between the use of sufficiently large samples to obtain repeatable results and not too large to still have a versatile and easy to move test.

This paper will present, in a first part, the dimensioning and operation procedure of the M-SBI test. Then, the test will be used to compare and to understand the fire behavior of rigid polyurethane foams (PUR) and rigid polyisocyanurate foams (PIR) that have been used as case study. These foams are formulated with and without FRs in order to study their impacts on combustion and flame propagation. Finally, the results obtained using the M-SBI test are compared with those collected in a widely used lab scale test, the mass loss cone test (MLC) to validate and demonstrate the relevance of our approach.

2. Experimental

2.1. Materials

Insulative foams are provided by BASF. Two types of foams are used in this study and prepared with and without FRs (**Table 1**).

Table 1: Weight percentage of chlorine, bromine and phosphorus contained within each system.

System	Cl (wt%)	Br (wt%)	P (wt%)
Foam 1 with FRs (PIR)	1.1	0.0	0.3
Foam 2 with FRs (PUR)	2.9	4.9	1.1

Foam 1 is a rigid polyisocyanurate prepared with a polyether polyol and a polymeric methylene diphenyl diisocyanate (PMDI). Additional additives are also used like stabilizer, catalyst, chemical and physical blowing agent. Apparent density is close to 39 kg.m^{-3} and the percentage of the closed cell content is near to 93 %. The closed cell content is determined with a gas displacement pycnometer (EN ISO 4590). In Foam 1 with FRs, the NCO/OH ratio is kept constant as well as the apparent density. This foam contains FRs that amount to a

final elemental content of 0.3 wt% phosphorus and 1.1 wt% chlorine. Foam 2 is a rigid polyurethane foam formulated with a polyether polyol and a PMDI. Additional additives are also used like stabilizer, catalyst, chemical and physical blowing agent. Apparent density is close to 39 kg.m^{-3} and closed cell content near to 91 %. Foam 2 contains FRs that amount to a final elemental content of 1.1 wt% phosphorus, 2.9 wt% chlorine and 4.9 wt% bromine. Panel size of foams supplied by BASF is $50 \text{ cm} \times 50 \text{ cm} \times 4 \text{ cm}$.

In general, the materials tested in the SBI test are in their final configuration of use, i.e. the materials may have air gaps, bolts, aluminum layer or joints. In the case of the M-SBI test, it is also possible to use materials in their final configuration of use. However, in the case of this study, only the foam will be studied and not the end-use configuration.

2.2. Mass loss cone

A mass loss cone (MLC) from Fire Testing Technology (FTT) was used to compare combustion results obtained with the M-SBI test. The procedure followed for these tests is described in ASTM E 906 or ISO13927 [17,18]. Thermopiles in the chimney, previously calibrated with methane, are used to determine the HRR. A sample of $10 \text{ cm} \times 10 \text{ cm} \times 4 \text{ cm}$ is placed on a support located directly on a scale. The sample is set up at 25 mm from a conical heater that generates a heat flux of 35 kW.m^{-2} . In order to define the radiative flux used, preliminary tests were carried out with a flux of 35 kW.m^{-2} and 50 kW.m^{-2} on similar systems with and without FRs. The values obtained were slightly different due to the variation of the irradiance; however, the trends were identical. Therefore, the value of 35 kW.m^{-2} was defined as the one indicated in the cone calorimeter ISO 5660 standard, which recommends an irradiance value of 35 kW.m^{-2} for exploratory testing. A spark igniter is placed above the sample to ignite the foam. The test is thus performed under forced ignition. A smoke density device with light measurement supplied by NETZSCH Taurus Instruments (model TRDA) is added at the exit of the chimney to determine the smoke release rate during combustion.

Regarding MLC test, the methane calibration of the thermopiles for the HRR measurements is known to lead to inaccuracies in the order of 25 % when the setup is used to test samples that produce bright flames [19]. However, the level of inaccuracy remains the same when comparing materials of the same nature. Thus, in order to avoid these problems even if the PIR and PUR structures show some similarity, only comparisons between systems of the same nature will be carried out. More precisely, comparisons between PUR systems (with and without FRs) will be possible as well as comparisons between PIR systems (with and without FRs).

2.3. M-SBI fire test

2.3.1. Setting

Figure 1 shows a general scheme and a picture of the M-SBI. This test is placed in a closed room exclusively dedicated to fire tests.

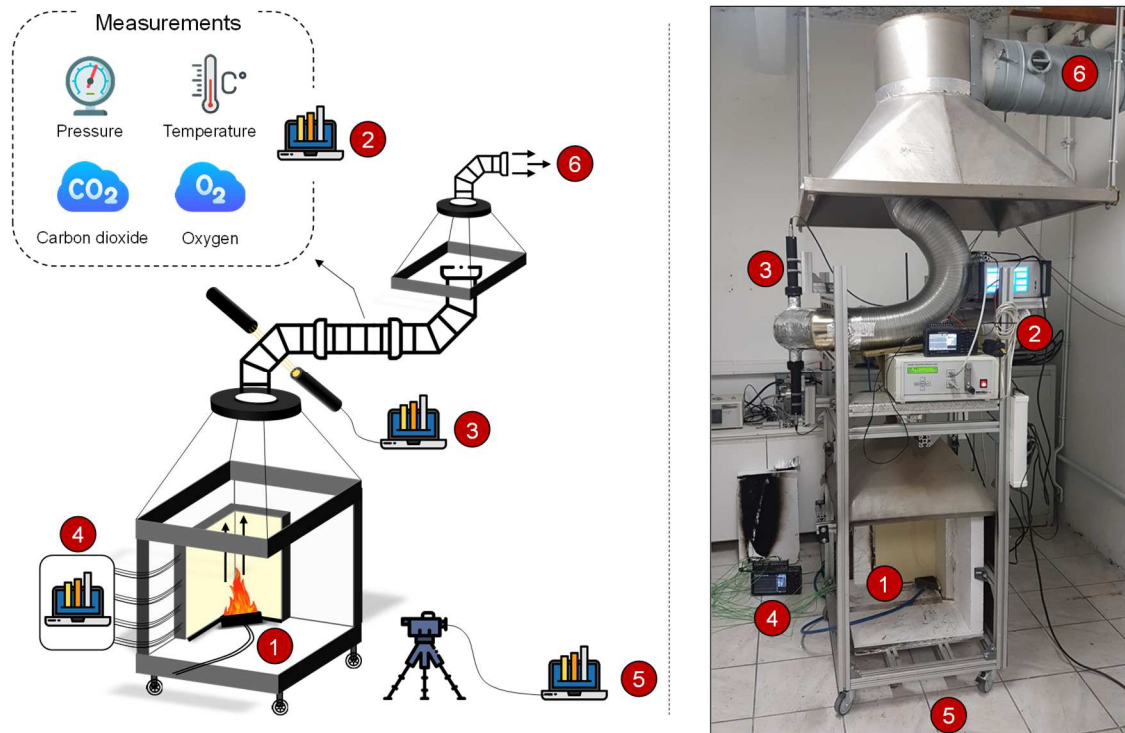


Figure 1: Scheme and image of the experimental device: the M-SBI. (1) Removable frame containing the panels and the burner, (2) Measuring tube, (3) Light sensors for smoke measurement, (4) 14 type K thermocouples, (5) Video camera, (6) Extractor hood.

The frame of the equipment (**Figure 1**, (1)) allows the attachment of the different elements necessary for the proper functioning of the test, such as the burner and the samples (small and large panels). Additional thermocouples (**Figure 1**, (4)) can be set up in the panels during the preparation of the samples.

A video camera (**Figure 1**, (5)) allowing visual observation of the combustion process is used. The camera is placed one meter away from the panels. The removable frame is surmounted by an exhaust duct where all the sensors are located (**Figure 1**, (2)). The light sensors (**Figure 1**, (3)) are used to measure the amount of smoke released during the decomposition of the material. The light rays pass through the diameter of the duct. Finally, the exhaust duct is connected to an extractor hood (**Figure 1**, (6)) with a constant extraction rate of $211 \text{ m}^3 \cdot \text{h}^{-1}$.

2.3.2. Detectors and analyzers

The M-SBI test is composed of a measuring exhaust duct containing several sensors (**Figure 1**, (2)) allowing the calculation of FIGRA and SMOGRA. The duct contains one thermocouple (type K with a diameter = 0.5 mm), a bi-directional probe purchased from Fire Testing Technology ($k_p = 1.08$) connected to a pressure sensor and an oxygen but also carbon dioxide analyzer constituted by a zirconia oxygen sensor (XGA301 from Michell Instruments).

A smoke density device with light measurement supplied by NETZSCH Taurus Instruments is used to characterize the smoke released during a test. The light emitter sensor is composed of a 10W halogen light source and tempered with heatproof optics. The light receiver sensor is constituted of silicon photo receiver, also tempered and with heatproof optics. A spectral filter and measuring light amplifier are also added.

2.3.3. Dimensions of the test

Figure 2a shows a more detailed image of the removable frame. The frame is equipped with wheels (**Figure 2a**, (2)) for an easier set-up. The propane inlet (**Figure 2a**, (1)) is directly connected to the burner. The propane used for the test has a purity of 95 %. The burner (**Figure 2a**, (3)) has a triangular shape prism and is a replica of the 1/3 scale SBI burner with the dimensions: 8.3 cm × 8.3 cm × 11.7 cm and a 2.6 cm height. A profile (**Figure 2a**, (4)) is used to create a small gap (1.3 cm) between the burner and the material to avoid direct contact of the burner with the panels like in the SBI test. The frame (**Figure 2a**, (5)) is made of three calcium silicate thermally resistant plates.

To verify that the downscaling did not impact the incident heat flux densities (kW.m^{-2}) of the burner, the heat flux has been quantified according to the SBI standard (annex D2). The measurements were performed on the required locations proportionally to the downscaling. In other words, three holes were drilled in a calcium silicate plate corresponding to the large plate and placed in the corner of the test. The three holes have the following position:

- Position 1: 2.7 cm from the corner and 5.3 cm from the top of the burner
- Position 2: 2.7 cm from the corner and 25 cm from the top of the burner
- Position 3: 6.7 cm from the corner and 10 cm from the top of the burner

The serie of tests showed a repeatability of the incident heat flux of 4 % and less, in accordance with the required limits. The position 1 presents an average heat flux of $29.1 \pm 0.86 \text{ kW.m}^{-2}$ (2.95 % relative standard deviation), the position 2 shows an average heat flux of $8.75 \pm 0.31 \text{ kW.m}^{-2}$ (3.62 % relative standard deviation) and the position 3 shows an average heat flux of $11.2 \pm 0.29 \text{ kW.m}^{-2}$ (2.58 % relative standard deviation).

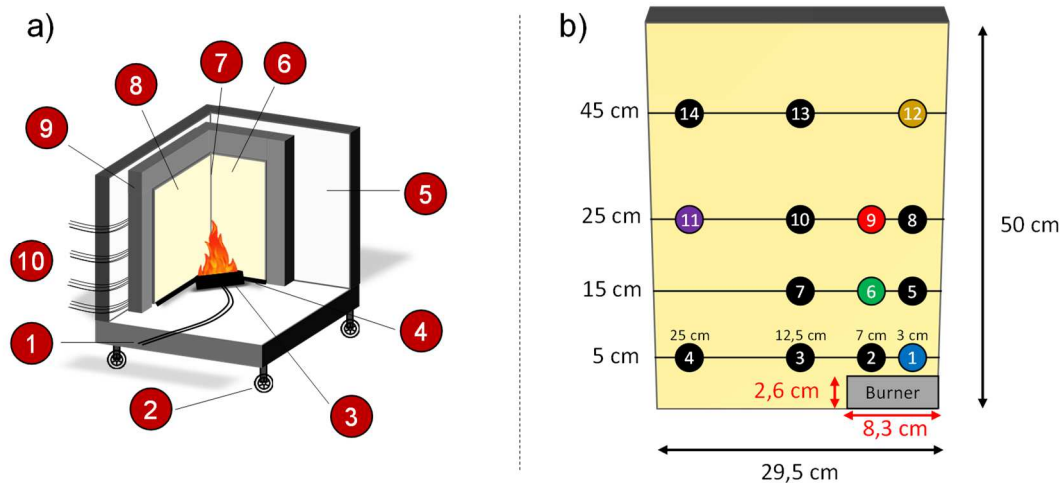


Figure 2: a) Scheme and image of the removable frame. (1) Propane inlet, (2) Wheels for the removable frame, (3) Burner, (4) U-profile separating the burner from the panel, (5) Calcium silicate plate, (6) Small panel, (7) Physical joint, (8) Large panel, (9) Steel structure, (10) 14 type K thermocouples in the large panel. b) Localization of the 14 thermocouples into the large panel.

2.3.4. Sample preparation

The panel used in the M-SBI test have the following dimensions: the large panel (**Figure 2a**, (8)) is 50 cm × 29.5 cm × 4 cm and the small panel (**Figure 2a**, (6)) is 50 cm × 20.5 cm × 4 cm. Concerning the setup, the small panel is first placed in the corner and then the large panel is placed on top of the small one. Thus, the large panel has an exposure width of 29.5 cm compared to 16.5 cm for the small one. The two panels are physically joined (**Figure 2a**,

(7)) to minimize air intakes and to prevent the flame from passing through. Then, a metal structure (**Figure 2a**, (9)) is positioned laterally and above the panels in order to lock them against the calcium silicate panels. The metal structure is placed to prevent flame propagation at the edges and therefore behind the material. Finally, thermocouples (**Figure 2b**) are placed in the sample. Type K thermocouples (diameter = 0.5 mm) are used for the core thermal mapping and are located 2 cm deep in the largest panel at specific locations in order to obtain optimal mapping during combustion. For this type of material, i.e. polyurethane or polyisocyanurate foams, the thermocouples are added by hand by the back of the panel. All the thermocouples, once placed in the foam are maintained with aluminum tape on the back of the sample. There are 3 to 4 thermocouples set up at four different heights.

2.3.5. Acquisition procedure

The procedure of the large-scale SBI test (EN13823) [8] is divided into four steps (**Figure 3**). The first one (I) lasts 120 seconds and corresponds to the acquisition of the baseline measurements when the burner is off. During the second step (II), from 120 s up to 300 s, the burner is switched on allowing the flame to stabilize. From 210 s to 270 s (step III) the calculation and calibration of the heat flux and smoke production of the burner are performed. This calibration lasts 60 seconds. Steps two (II) and three (III) necessitate the use of an auxiliary burner. Finally, at 300 s (step IV), the auxiliary burner is switched off and the main burner is turned on; the panel combustion starts and lasts 1260 s. The characteristic data obtained from the experiment are heat release, smoke release, lateral propagation of the flame front and presence of droplets and of flaming particles.

A similar approach was set up in the case of M-SBI test, except that the burner calibration is not performed with an auxiliary burner but with the same burner previously described (**Figure 2a**, (3)). The calibration is performed with blank calcium silicate panels, which are replaced by the sample to be tested when the data acquisition is performed. The power of the burner was set up at 1.51 kW (compared to 30.7 kW for the standard burner). Based on Froude modeling principles [9], the burner power should have been set at 1.97 kW. However, preliminary tests showed that the obtained flame size was too large, causing quickly the combustion of the top edge and of the back of the sample, prohibiting a good discrimination of the samples. For this reason, the power was reduced down to 1.51 kW.

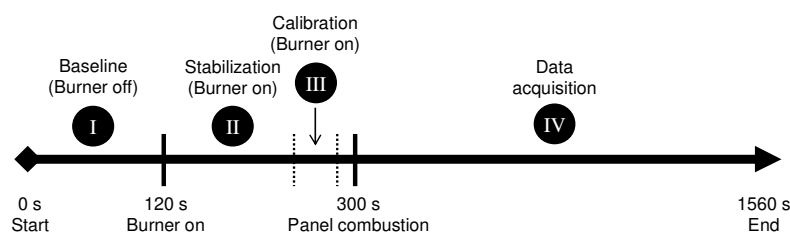


Figure 3: Procedure of use for the SBI and M-SBI.

3. Results and discussion

3.1. Optimization of the procedure

3.1.1. Baseline and calibration (heat release)

Baseline measurement and burner calibration are performed at the beginning of each test. This part of the paper highlights the accuracy of the repeatability of the baseline

measurement and burner calibration. Thus, the values presented hereinafter are the results of a series of five tests carried out on the same day. As described in part 2.3.5, the baseline measurement and calibration lasts 300 seconds and is divided into three steps. The first step (120 s without burner) allows to measure a number of parameters that are required to determine the main data of the test (FIGRA and SMOGRA). During the first step (I), the oxygen and carbon dioxide content in the exhaust duct, its temperature, the variation of pressure as well as the relative humidity (RH) and the temperature of the room are collected. The average values corresponding to a series of 5 trials are given in **Table 2**.

Table 2: Baseline measurements of O₂, CO₂, temperature in the duct, pressure variation, relative humidity and room temperature from 0 s to 120 s.

	O ₂ (vol.-%)	CO ₂ (ppm)	T _{duct} (°C)	ΔP (Pa)	RH _{room} (%)	T _{room} (°C)
Average	21.02	568	16.7	12.6	75	16.7
Std. dev.	0.01	10	0.2	0.6	/	/

The oxygen concentration was around 21.02 vol.-% and the carbon dioxide concentration was around 568 ppm. The temperature in the duct was 16.7°C and similar to the room temperature (16.7°C). The variation of pressure was around 12.7 Pa. The relative humidity of the room was 75 %. These parameters obviously vary depending on the day the M-SBI test is used and will be determined at the beginning of each trial.

The second and third steps (from 120 s to 300 s) are dedicated to the burner calibration. The flame is allowed to stabilize for 90 seconds (from 120 seconds to 210 seconds) and the data are acquired between 210 seconds and 270 seconds (**Table 3**).

Table 3: measurements of O₂, CO₂, temperature in the duct, pressure variation, relative humidity, room temperature and calculation of the heat release rate from 210 s to 270 s (III).

	O ₂ (vol.-%)	CO ₂ (ppm)	T _{duct} (°C)	ΔP (Pa)	RH _{room} (%)	T _{room} (°C)	HRR (kW)
Average	20.88	1292	24.6	12.7	75	16.7	1.52
Std. dev.	0.01	45	0.3	0.6	/	/	0.13

As soon as the burner is in operation, the concentration of oxygen decreases from 21.02 vol.-% to 20.88 vol.-% in the duct since oxygen is consumed by the combustion of propane. Conversely, the concentration of carbon dioxide increases from 568 ppm to 1292 ppm since there is production of CO₂ due to propane combustion. Moreover, due to convective effect, the temperature increases in the measuring duct from 16.7°C to 24.6°C.

As a reminder, the objective is to show that the burner calibration values are relatively repeatable over the trials. Moreover, the purpose of the burner calibration is to be able to later subtract this value from the total amount of energy released during the combustion of the panels in order to know precisely the heat release of the materials during the test. In order to be able to access the actual HRR values of the burner (**Equation 1**), the normalized extraction flow (V_{298K}), the volume concentration of oxygen in ambient air (x_{a,O_2}) and the oxygen consumption factor ($\Phi(t)$) are needed.

$$HRR(t) = E \cdot V_{298K}(t) \cdot x_{a,O_2} \cdot \left(\frac{\Phi(t)}{1 + 0.105\Phi(t)} \right) \quad \text{Equation 1}$$

HRR (t): heat release rate (kW)

E: energy released per volume of oxygen consumed at 298 K = 17200 kJ·m⁻³

$V_{298K}(t)$: normalized extraction flow at 298 K (m³·s⁻¹)

x_{a,O_2} : volume concentration of oxygen in ambient air, including water vapor

$\Phi(t)$: oxygen consumption factor

The calculation of x_{a,O_2} and $\Phi(t)$ are straightforward and explained in details in the SBI standard (EN13823) [8]. V_{298K} is calculated using **Equation 2**.

$$V_{298K}(t) = c \cdot A \cdot \frac{k_t}{k_\rho} \cdot \sqrt{\frac{\Delta P(t)}{T_{duct}(t)}} \quad \text{Equation 2}$$

$V_{298K}(t)$: normalized extraction flow at 298 K ($m^3 \cdot s^{-1}$)

$c = 22.4 K^{0.5} \cdot m^{1.5} \cdot kg^{-0.5}$

A : section of the measuring tube in the extraction duct = $1.8 \cdot 10^{-2} m^2$

k_t : flow form factor = 0.742

k_ρ : Reynolds correction coefficient for the bi-directional probe = 1.08

$\Delta P(t)$: pressure variation (Pa)

$T_{duct}(t)$: temperature in the general measuring tube (K)

The coefficient flow profile (k_t) has been determined taking into account the use of a burner power set up at 1.51 kW. A series of preliminary tests was carried out by setting the propane flow rate to $0.12 kg \cdot h^{-1}$, i.e. corresponding to a theoretical HRR of 1.51 kW allowing to obtain an average value of k_t equal to 0.742. The normalized extraction flow (V_{298K}) does not vary significantly during the entire burner calibration and is close to $211 m^3 \cdot h^{-1}$.

After the 5 trials performed, the average HRR of the burner can be calculated with **Equation 1**. The average HRR calculated between 210 s and 270 s is equal to 1.52 ± 0.13 kW (**Figure 4**). This value is close to the theoretical HRR calculated for a propane flow rate of $0.12 kg \cdot h^{-1}$ (red line in **Figure 4**). In conclusion, the mean value and its standard deviation over 5 trials (1.52 ± 0.13 kW) show that the repeatability and the accuracy are good.

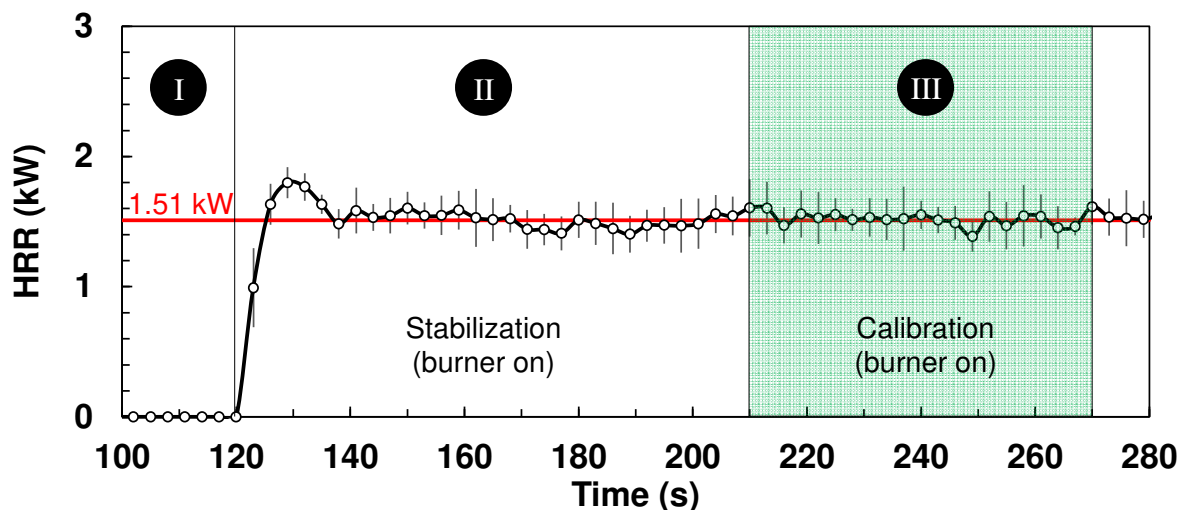


Figure 4: Measurement of the HRR during the baseline (I) and burner calibration (II and III). Error bars indicate the scatter over the five trials conducted.

3.1.2. Baseline and calibration (smoke release)

Smoke measurement is also performed during the M-SBI test. The calibration of the light transmission is performed at the same time as the calibration of the HRR data (steps I, II and III). These average values corresponding to the same series of 5 trials as for the heat release calibration are presented in **Table 4**. **Figure 5** shows the evolution of the smoke production rate (SPR) versus time but also versus the different steps of the M-SBI procedure

(I, II and III). The values of the light transmission measured between 0 s and 120 s (I) correspond to the step without any flame and thus a set value at 100 %. Between 120 s and 300 s (II and III), the burner is turned on and smoke is released from the combustion of propane. The combustion of propane causes a slight appearance of smoke, which decreases the light transmission from 100.07 % to 99.41 %. Therefore, the SPR can be calculated using the **Equation 3**.

$$SPR(t) = \frac{V(t)}{L} \cdot \ln \left[\frac{\bar{I}_{30s\ to\ 90s}}{I(t)} \right] \quad \text{Equation 3}$$

SPR (t): smoke production rate ($\text{m}^2 \cdot \text{s}^{-1}$)

V (t): non-normalized extraction flow

L: length of the light path through the general measuring tube = 0.153 m

$\bar{I}_{(30\ s\ to\ 90\ s)}$: average value from 30 s to 90 s of the light transmission (%)

I (t): opacimeter output signal (%)

Consequently, the SPR increases from 0 to $25.9\ \text{cm}^2 \cdot \text{s}^{-1}$. In conclusion, the mean value and its standard deviation over 5 trials ($25.9 \pm 0.13\ \text{cm}^2 \cdot \text{s}^{-1}$) show that the repeatability and the accuracy are good.

Table 4: Smoke baseline from 0 s to 120 s (I) and smoke measurement of light transmission from burner calibration from 210 s to 270 s (II and III).

System	Light transmission (%)	SPR ($\text{cm}^2 \cdot \text{s}^{-1}$)
Average (0 s to 120 s)	100.07	0
Std. dev.	0.02	0
Average (210 s to 270 s)	99.41	25.9
Std. dev.	0.10	3.2

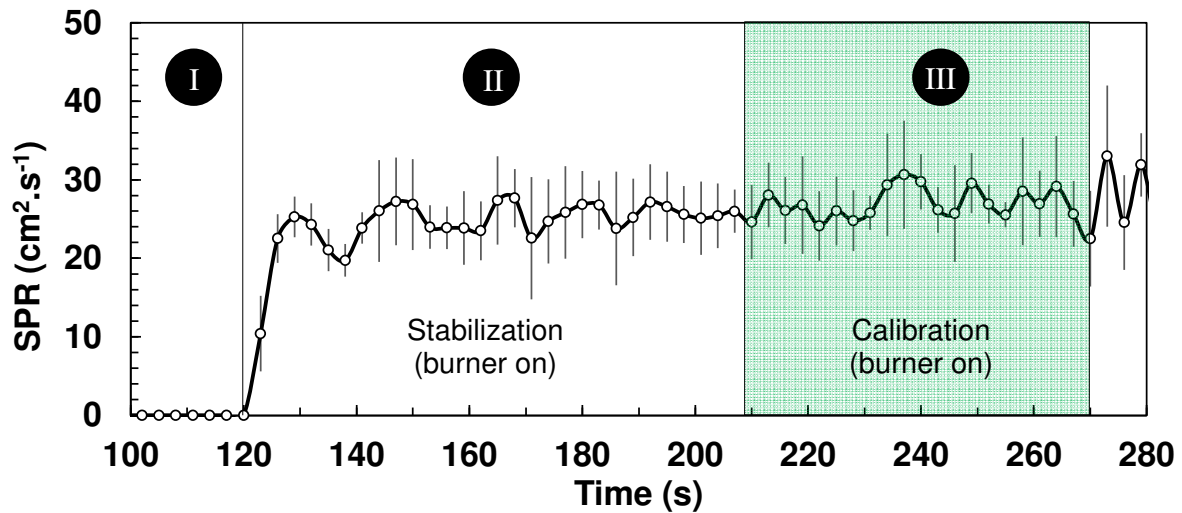


Figure 5: Measurement of the SPR during the baseline (I) and burner calibration (II and III). Error bars indicate the scatter over the five trials conducted.

3.1.3. Combustion of the sample (Data acquisition)

The step four (IV) consists in the measurement of the combustion parameters of the sample when tested. It lasts 1260 seconds as in the standard. At the beginning of this step, the panels are set up in the corner and the burner is switched on for 1260 seconds. As soon as the burner is in contact with the sample, the data (oxygen and carbon dioxide concentration, temperature in the exhaust duct, variation of pressure, room temperature,

relative humidity of the room and light transmission) are collected. From those data, the $HRR_{av(30\ s)}$ corresponding to the average of the HRR values over 30 seconds, the total heat release (THR) and the FIGRA corresponding to the ratio between the heat release rate measured at a given time t and the time t (**Equation 4**) are determined.

$$FIGRA = 1000 \times \max \cdot \left(\frac{HRR_{av(30\ s)}(t)}{t - 300} \right) \quad \text{Equation 4}$$

The FIGRA ratio is only calculated if the threshold values are exceeded during the whole test period, that is to say, a HRR higher than 0.15 kW and a THR higher than 0.01 MJ. These threshold values have been adjusted for the M-SBI test. Indeed, these threshold values have been reduced by a factor of 20.3 corresponding to the downscaling of the power of the burner from 30.7 kW (SBI) to 1.51 kW (M-SBI). Two particular values are defined: $FIGRA_{0.02\ MJ}$ corresponding to the value of FIGRA when THR reaches a value of 0.01 MJ and $FIGRA_{0.04\ MJ}$ corresponding to the value of FIGRA when THR reaches a value of 0.02 MJ. The unit of FIGRA is given in $W \cdot s^{-1}$.

From the collected data, the $SPR_{av(60s)}$ (corresponding to the average of the SPR values over 60 seconds) is calculated but also the total smoke production (TSP) and the smoke growth rate index (SMOGRA) corresponding to the speed of development of the smoke. SMOGRA corresponds to the ratio between the rate of smoke production at a given time t and the time t (**Equation 5**). The unit of SMOGRA is given in $cm^2 \cdot s^{-2}$.

$$SMOGRA = 10000 \times \max \cdot \left(\frac{SRR_{av(60s)}(t)}{t - 300} \right) \quad \text{Equation 5}$$

Like the FIGRA index, the SMOGRA index ratio is only calculated if the threshold values are exceeded during the whole test such that a SPR higher than $50\ cm^2 \cdot s^{-1}$ and a TSP higher than $0.3\ m^2$. In the same way, the threshold values presented have been adapted to fit the M-SBI test.

3.2. Application to the case studies

3.2.1. Heat release and flame propagation

The first system studied in this paper is the PIR (Foam 1) with and without FRs (0.3 wt% phosphorus and 1.1 wt% chlorine for the PIR with FRs). **Figure 6a**, **Figure 6b** and **Figure 6c** show the evolution of the different parameters measured during the combustion of polyisocyanurate systems. **Figure 6d** shows the evolution of the $HRR_{av(30\ s)}$ from 0 s to 1500 s to fit with the SPR_{60s} . Finally, the **Figure 6e** presents the evolution of the THR and of the fire growth rate index (FIGRA) from 300 s (start of panel burning) up to 900 s.

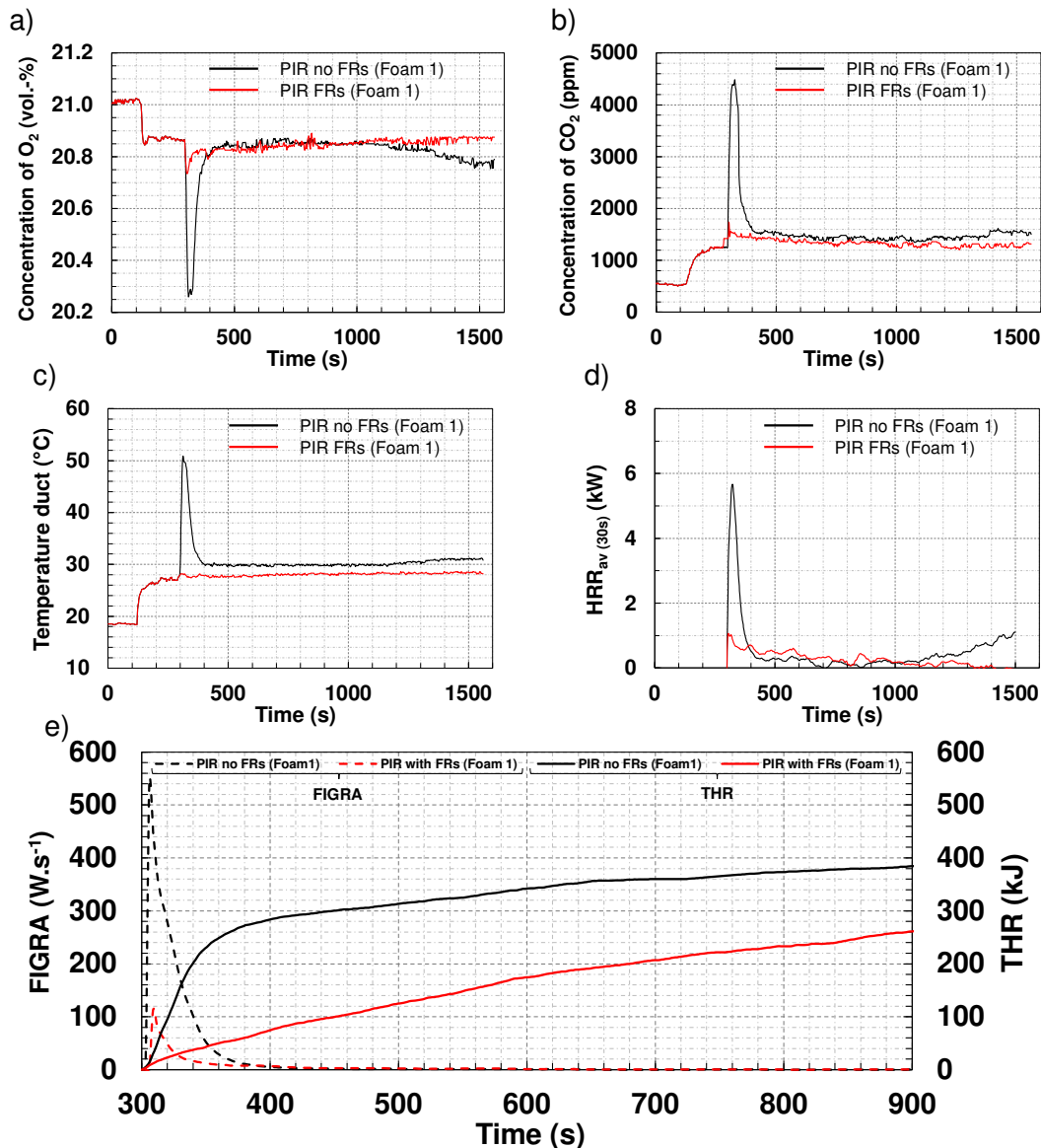


Figure 6: Evolution of the concentration of O₂ (a), concentration of CO₂ (b), temperature of the duct (c), HRR_{av(30s)} (d), THR (e) and FIGRA (e) during the combustion of the PIR systems (with and without FRs).

In the case of PIR without FRs, oxygen consumption decreases sharply to reach a minimum of 20.26 vol.-% at 312 s, i.e. almost immediately after the panel was put in contact with the burner. Conversely, the PIR with FRs presents a better behavior by showing a smaller decrease in the oxygen consumption since the minimum is equal to 20.74 vol.-% at 306 s. Generally speaking, the stronger the combustion, the higher the oxygen consumption and the higher the carbon dioxide flowrate and temperature in the extraction duct. This trend is also observed in **Figure 6b**. The maximum carbon dioxide release reaches 4487 ppm for the PIR without FRs versus 1720 ppm for PIR with FRs. Due to stronger combustion, PIR without FRs leads to a temperature of 50.9°C in the duct versus only 28.2°C for the PIR with FRs. As a direct consequence, the HRR_{av(30 s)} is higher without FRs (5.67 kW at 324 s) compared to PIR with FRs (1.06 kW at 306 s). The M-SBI test clearly demonstrates that FRs significantly modify the combustion phenomenon and reduce the combustion intensity when a burner power of 1.51 kW is applied. In the case of PIR without FRs, the HRR_{av(30 s)} increases slightly from 1200 s, which is due to the penetration of the flame into the material causing again a slight combustion of the material. The THR is always lower in the case of the

PIR with FRs over the time and shows a much lower fire growth rate (FIGRA) than the system without FRs.

In order to complete these measurements, a video camera is set up and records the whole experiment. Images recorded at several combustion times are displayed in **Figure 7**. They allow to show the difference in combustion intensity as a function of time. At 310 s (10 s after the contact between the burner and the foam), the combustion of PIR without FRs is more intense and goes far beyond the metal protective frame over the foam panels. At 330 s, lateral flame spread is observed for PIR without FRs, whereas the combustion intensity does not vary visually on PIR with FRs. At 900 s and 1560 s, the combustion in both cases (with and without FRs) appears identical. The char formed during the first phase of combustion protects the core of the foam and strongly reduces or even completely stops the combustion of the panel.

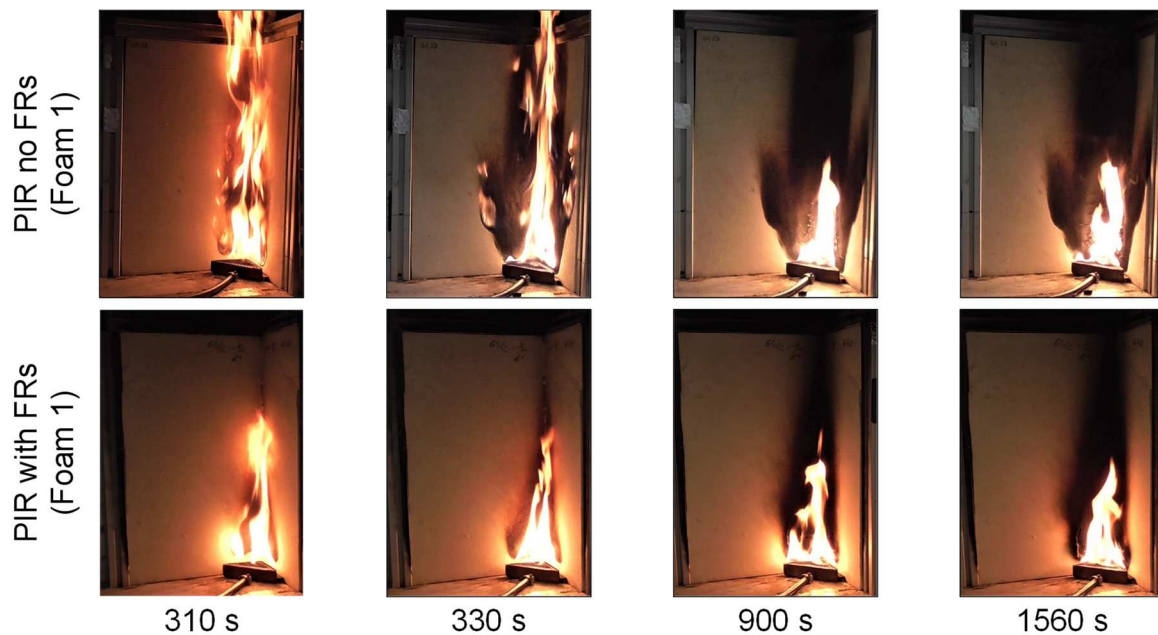


Figure 7: Visual observation of the polyisocyanurate system (PIR) with and without FRs between 300 s (start of panel combustion) and 1560 s (end of test).

Concerning PIR with and without FRs, the observation of all the parameters but also the visual observation clearly show the impact of FRs on the combustion phenomenon and show the interest to use FRs in order to limit the spread of a fire.

The second system studied is the foam 2 corresponding to rigid polyurethane foam (PUR) with and without FRs. Unlike polyisocyanurate, polyurethane has a chemical structure less thermally stable and is more prone to thermal decomposition [20]. That is why the amount of FRs used is often higher. As a reminder, the system is available into two variants, a virgin product with no FRs and another containing 1.1 wt% of phosphorus, 2.9 wt% of chlorine and 4.9 wt% of bromine. **Figure 8a**, **Figure 8b** and **Figure 8c** show the evolution of the parameters measured during the combustion of PUR systems. **Figure 8d** and **Figure 8e** present the $HRR_{av(30\ s)}$, THR and FIGRA, respectively.

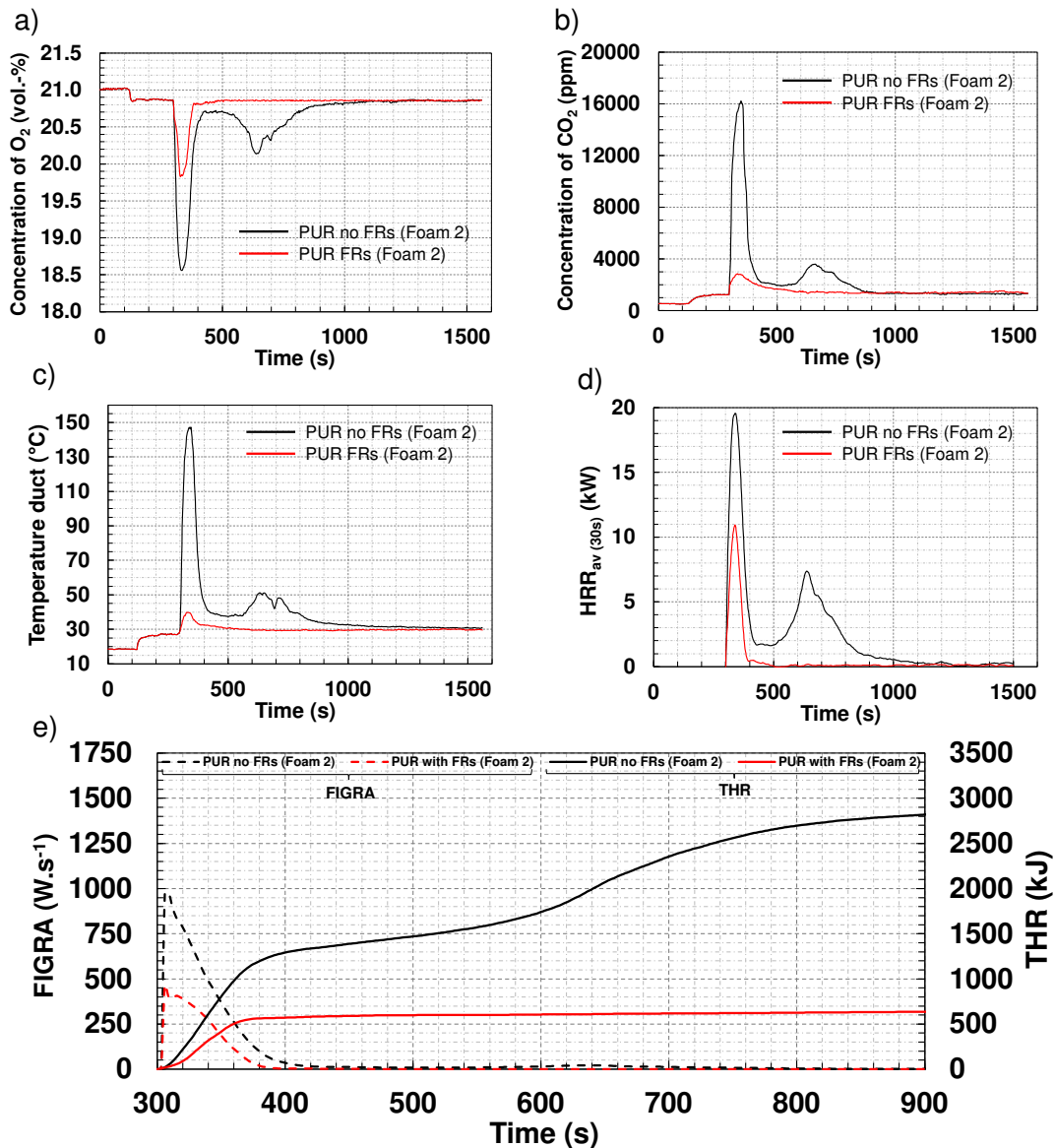


Figure 8: Evolution of the concentration of O₂ (a), concentration of CO₂ (b), temperature of the duct (c), HRR_{av(30s)} (d), THR (e) and FIGRA (e) during the combustion of the PUR systems (with and without FRs).

Similarly to what was observed for PIR foam, in the case of the PUR without FRs, the oxygen consumption decreases very significantly with a minimum of 18.56 vol.-% at 336 s, i.e. few seconds after the panels are put in contact with the flame of the burner. The maximum carbon dioxide release is 16220 ppm for the system without FRs compared to 2860 ppm for system with FRs. Regarding the temperature in the duct, it reaches 147.2 °C for PUR without FR compared to 39.8°C for PUR with FRs. Finally, the HRR_{av(30 s)} curve shows that PUR without FRs burns more vigorously (the maximum is equal 19.6 kW at 336 seconds) than PUR with FRs (the maximum value is equal to 10.9 kW at 339 seconds). These values are significantly higher than those obtained in the case of the PIR systems, showing the difference in the combustion rate for both systems confirming that polyisocyanurate are more thermally stable than polyurethane foam. In the case of PUR without FRs, the HRR_{av(30 s)} increases again after 500 s and a second peak is noted. This phenomenon is due to the flame propagation behind the panel through the upper edge of the panel. **Figure 8e** also shows the evolution of the total heat release (THR) and the FIGRA from 300 s (start of panel burning) to 900 s. The THR is always lower in the case of PUR with FRs over the time and shows a much lower fire growth rate (FIGRA) than the system without

FRs. Regarding PUR without FRs, two successive increases in THR can be observed. The first increase corresponds to the first combustion of the panel with lateral flame spread between 300 s and 400 s and the second from 560 s up to about 760 s corresponding to the combustion at the back of the panels.

Compared to PIR systems, which do not exhibit strong flame spread, visual observations of PUR systems at different combustion times show the strong impact of FRs on the lateral spread of the flame and on the intensity of combustion (**Figure 9**). The system without FRs shows extremely strong combustion at 310 s with fast lateral flame spread at 330 s. Flame spread is almost complete on the largest panel at about 360 s. The combustion is so powerful that the flame extends beyond the metal frame. The flame then decomposes the upper edge of the material and allows the flame to penetrate the back of the panel. Thus, as soon as the combustion in front of the panel is stopped, a new combustion takes place close to the top of the panel and at the back. This observation is possible at 638 s. This secondary combustion will stop by itself what can be observed at around 1100 s (**Figure 8d**). Thus, the use of FRs in this system initially avoids the lateral propagation of the flame and as a consequence, strongly reduces the intensity of the combustion. Indeed, the flames barely exceed the metal structure that supports the foam panels.

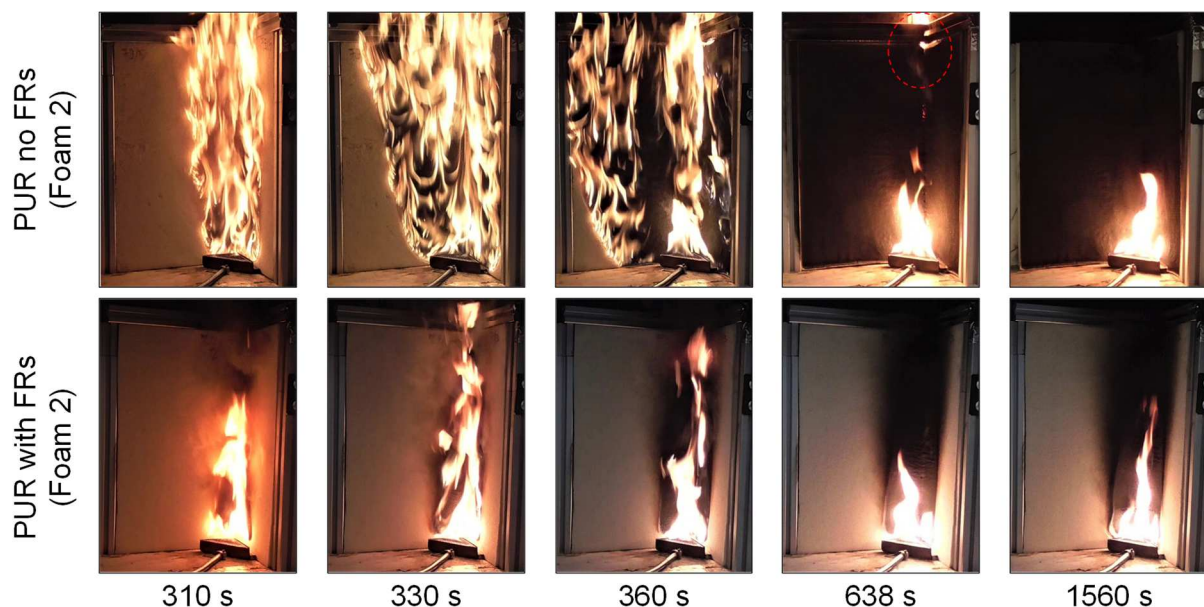


Figure 9: Visual observation of the polyurethane system (PUR) with and without FRs between 300 s (start of panel combustion) and 1560 s (end of test).

Table 5 gathers the data mainly used in the standard and collected with the M-SBI test. The peak $HRR_{av(30\ s)}$ represents the maximum value of energy released during combustion and the THR_{600s} presents the total energy value released between 300 s and 900 s. From the FIGRA point of view, the values presented in the original standard correspond to $FIGRA_{0.2\ MJ}$ and $FIGRA_{0.4\ MJ}$. However, due to downscaling, the FIGRA limit values have been adapted and are now $FIGRA_{0.01\ MJ}$ and $FIGRA_{0.02\ MJ}$ (as explained in part 3.1.2.). Finally, the lateral flame spread is measured and corresponds to the maximum distance the flame has reached on the largest panel. The lateral flame spread is presented in cm and in percentage in relation to the exposure width.

Table 5: Main data calculated with M-SBI test for PIR (foam 1) and PUR (foam 2) systems.

System	Peak $HRR_{av(30\ s)}$ (kW)	$THR_{600\ s}$ (kJ)	$FIGRA_{0.01\ MJ}$ ($W.s^{-1}$)	$FIGRA_{0.02\ MJ}$ ($W.s^{-1}$)	Lateral propagation (cm)
PIR no FRs	5.7	385	542	449	15.7 (53.2%)
PIR FRs	1.1	261	113	57	10.9 (36.9%)
PUR no FRs	19.6	2818	975	975	29.5 (100.0%)
PUR FRs	10.9	636	460	406	9.8 (33.2%)

In both systems, PIR and PUR, the use of FRs allows to improve the fire properties of the material, reducing the peak $HRR_{av(30\ s)}$, $THR_{600\ s}$ as well as the $FIGRA_{0.01\ MJ}$ and $FIGRA_{0.02\ MJ}$. For example, for PIR with FRs, the peak $HRR_{av(30\ s)}$ is decreased by 81 %, the $THR_{600\ s}$ by 32 % and the $FIGRA_{0.01\ MJ}$ by 87 %. As mentioned above, PIR systems by nature have a chemical structure that is more resistant to thermal decomposition and therefore have a lower energy released during combustion ($THR_{600\ s}$ of virgin PIR is equal to 385 kJ compared to 2818 kJ for virgin PUR). In addition, the use of FRs avoids in both cases the lateral spread of the flame by reducing it by 16.3 % for the PIR system and by 66.8 % for the PUR system. The M-SBI system therefore highlights the action of flame-retardants on the intensity of combustion and on flame propagation.

3.2.2. Smoke production

Figure 10 shows the evolution of the smoke production rate (SPR) during the combustion of the different panels. In the case of the PIR systems, the use of FRs decreases the smoke production rate. Indeed, the peak of the $SPR_{av(60\ s)}$ observed for the virgin foam ($203\ cm^2.s^{-1}$) is much higher than the one for the material including flame retardant ($93\ cm^2.s^{-1}$). Regarding the virgin foam, from 1200 s, the $SPR_{av(60\ s)}$ increases due to the penetration of the flame into the material causing again a slight combustion of the material, as discussed previously considering the $HRR_{av(30\ s)}$. The total smoke production (TSP) is always higher whatever the time in the case of the foam without FRs. Finally, the flame retarded PIR foam shows a low $SMOGR_{max}$ ($0.9\ cm^2.s^{-2}$) contrary to its counterpart without FRs ($13.4\ cm^2.s^{-2}$). In other words, the maximum speed of smoke development is extremely low in the case of the flame retarded PIR foam and rather fast in the case of PIR foam without FRs.

On the contrary, it can be observed that the use of FRs greatly increases the rate of smoke released in the case of PUR. Indeed, the peak $SPR_{av(60\ s)}$ measured for the virgin PUR foam ($1141\ cm^2.s^{-1}$) is much lower than in the case of the foam with FRs ($2642\ cm^2.s^{-1}$). The smoke rate increases again after 560 s, which is due to the flame propagation on the upper edge of the material and in the back, as already described in the previous section. As opposed to PIR foams, TSP is always lower whatever the time in the case of the PUR foam without FRs. Moreover, the $SMOGR_{max}$ is extremely high in the case of the flame retarded PUR foam ($405\ cm^2.s^{-2}$).

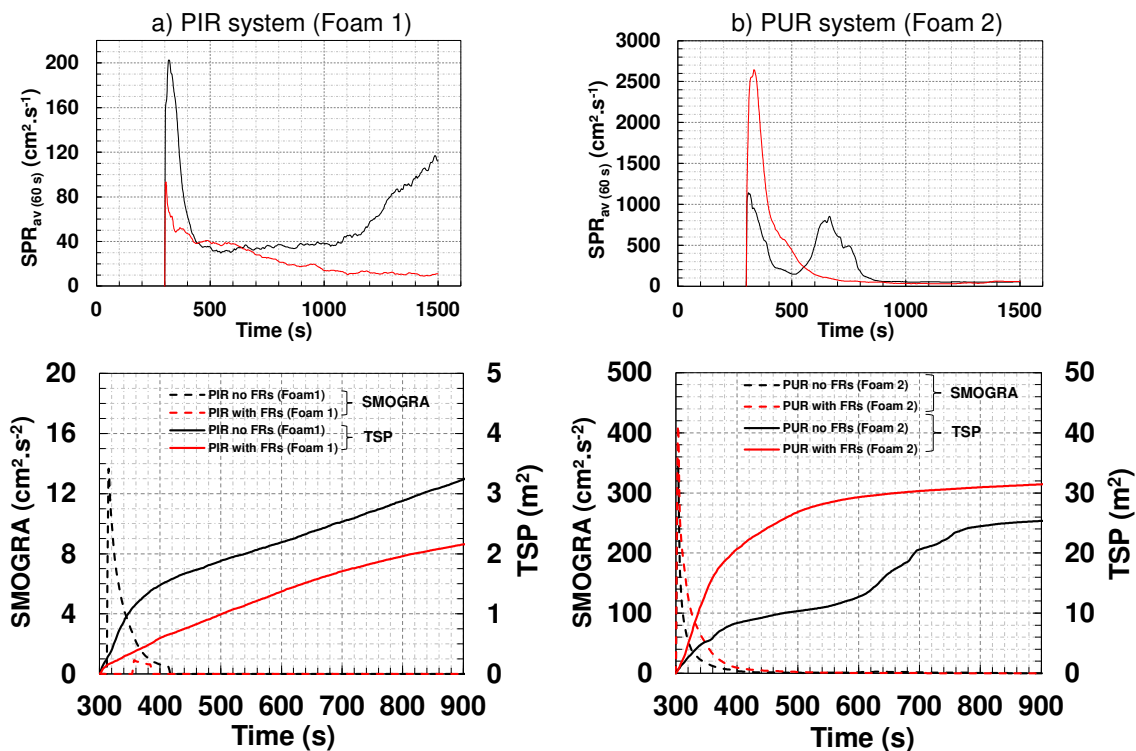


Figure 10: Smoke production rate ($SPR_{av(60 s)}$), TSP and SMOGRA for the a) polyisocyanurate system (PIR) and b) polyurethane system (PUR).

As a conclusion, **Table 6** presents the smoke production data obtained from the M-SBI tests based on **Equation 4** and **Equation 5**, following the methods described in the SBI standard (EN 13823). In the case of PIR, the addition of FRs in the formulation allows on the one hand to reduce the combustion rate, but also to reduce the rate of smoke produced. Indeed, the $SPR_{av(60 s)}$, THR_{600s} and SMOGRA are lower than for its virgin counterpart. On the other hand, the use of FRs in the PUR systems, which is much higher than the PIR system (1.1 wt% phosphorus, 2.9 wt% chlorine and 4.9 wt% bromine versus 0.3 wt% phosphorus and 1.1 wt% chlorine) increases the rate of smoke released during combustion. The TSP_{600s} increases by 24 % when using FRs.

Therefore, FRs greatly modify the fire behavior of the material and lead to many consequences on the HRR and SPR, which depend strongly on the nature of the material, the FRs used and the quantity of FRs. Indeed, in literature, Liu *et al.* demonstrate that the use of polymers with a chemical structure including aromatics in their backbone showed an increased thermal stability and consequently a reduction of smoke production during combustion [21]. They showed a direct relationship between the formation of the char and the rate of smoke emitted. Therefore, the more efficient the char formation is, the more the compounds from combustion are trapped in the condensed phase and the more the smoke rate decreases. The polyisocyanurate structures are made up of aromatic rings with a thermally stable three-dimensional network that promotes the reduction of smoke during combustion [22,23]. Thus, PIR foam without FRs has a TSP_{600s} almost 8 times lower than PUR foam without FRs. Now concerning the impact of the FRs used in both systems, their function is different. The FRs in the PIR system are chosen to promote charring of the material. This leads to a decrease in the peak $HRR_{av(30 s)}$, but at the same time reduces the smoke emission rate of the material. Conversely, the use of FRs for PUR foams is more centered on gas phase activity and increases the smoke formation rate even though the THR_{600s} is much lower than for the virgin system. The literature shows that the use of gas phase active flame retardants such as tris (1-chloro-2-propyl) phosphate (TCPP) or dimethyl

methyl phosphonate (DMMP) significantly increases smoke formation rate in PUR systems during combustion [21]. Indeed, PO[•] and Cl[•] radicals resulting from the decomposition of FRs will recombine with H[•] and OH[•] radicals (radicals causing the maintenance of the combustion) and prevent the phenomenon of oxidation and combustion [24,25]. Combustion is consequently incomplete and does not allow total oxidation of the evolved molecules. The increase in phosphorus oxides and fragments resulting from decomposition are greater in the gas phase, which increases the density of the smoke as well as the toxicity [26,27].

Table 6: Main results of smoke production data obtained using the methods described in the SBI standard (see Equation 4 and Equation 5). Comparison of the two systems with and without FRs.

System	Peak SPR _{av(60 s)} (cm ² .s ⁻¹)	TSP _{600s} (m ²)	SMOGR _{max} (cm ² .s ⁻²)
PIR no FRs	203	3.2	13.4
PIR FRs	93	2.2	0.9
PUR no FRs	1141	25.4	341
PUR FRs	2642	31.4	405

3.3. Additional data measurement: temperature mapping

One of the main advantages of using lab-scale testing method is the possibility to more easily use additional sensors to collect precious information, such as for example temperature mapping. Indeed, in the SBI test, the addition of thermocouples in the material is possible but not necessary to perform the test and validate its conformity. This kind of sensors enable the better understanding of foam behavior and thus allow to propose strategies to improve the fire behavior of materials. This approach was followed in our study and fourteen thermocouples were set up at different locations in the foam panels to build a temperature mapping. In order to facilitate the reading of the graphs and the understanding of the temperature evolution, the results of only five thermocouples have been presented (**Figure 11**). Thermocouples (1, 6, 9, 11 and 12) (**Figure 2b**) were selected. Thermocouples (1, 6, 9, 12) are located vertically to the flame at different heights. Thermocouple (11) is located at a height of 25 cm (same as thermocouple (9)) and 25 cm away from the burner. It allows to study the heat penetration during the propagation of the flame.

Figure 11 shows the evolution of the temperature for each thermocouple (1, 6, 9, 11 and 12) as a function of time. In the case of the PIR system, the FRs decrease the power of combustion and consequently the temperature in the material. Thus, the temperature curves for each thermocouple in the fire-retarded PIR foam are always lower than their counterpart without FRs.

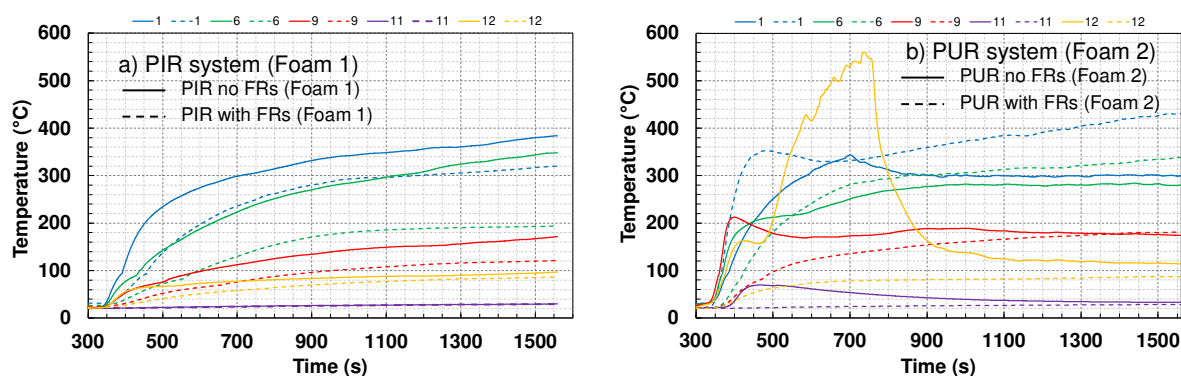


Figure 11: Evolution of the temperature at 2 cm depth in the core of PIR systems and PUR systems.

The temperature increase in the core of the PUR system is different. First, a few seconds after the application of the burner on the foam, the temperature increase directly above the burner (thermocouples 1, 6, 9 and 12) is much more significant for PUR foams than for PIR foams. This effect is more pronounced when no FRs are added. However, there is an exception for thermocouple 1 in the case of PUR with FRs. Indeed, the decomposition of the foam is more pronounced at this position, which causes a decrease in thickness and consequently a rapid increase of the temperature. Thermocouple 11 shows the evolution of the temperature due to the lateral propagation of the flame. At 500 s, it can be seen that a temperature of 68°C is reached for the PUR panel without FRs versus a temperature close to room temperature for the system with FRs. It demonstrates that in this case, the flame propagates quickly when no FRs are used. Finally, thermocouple 12 measures a very high temperature in the case of PUR without FRs, demonstrating the effect of the combustion at the back of the panel presented in **Figure 8d** and **Figure 9**.

In conclusion, the addition of a low amount of FRs in the PIR system reduces the combustion intensity, increases the charring and consequently decreases the heat transfer within the material. With respect to the PUR system, the addition of FRs (1.1 wt% phosphorus, 2.9 wt% chlorine and 4.9 wt% bromine) avoids lateral flame propagation and reduces the combustion intensity. However, it seems to decrease the thermal resistance and the charring efficiency of the material during prolonged contact with the flame of the burner (it can be only seen with the thermocouple 1 of the PUR system with FRs in **Figure 11**).

3.4 Comparison with mass loss cone test (MLC)

In order to validate the M-SBI heat and smoke measurements and to demonstrate the relevance of the use of such a testing method, the data obtained in this study are compared with the results obtained for the same materials using MLC test.

The MLC test is a bench-scale test traditionally used to determine the heat release rate of a material in the event of a fire. The smoke released can also be measured using a light beam at the chimney exit. The MLC measurement setting differs from the M-SBI test. Indeed, in the case of the MLC test, the sample size is smaller (10 cm × 10 cm × 4 cm versus 50 cm × 50 cm × 4 cm) and the whole sample is exposed to the heat source. Then, compared to M-SBI test, no lateral flame propagation on the material is considered, which allows discrimination of the fire behavior of the foams considered as case studies.

Figure 12 presents the evolution of HRR and TSP as a function of time for tests carried out on the mass loss cone under a heat flux of 35 kW.m⁻². Observation of the HRR curves shows that the use of FRs visibly decreases the peak HRR. The HRR curve also shows the two completely different trends between PUR and PIR. In fact, PUR without FRs shows a peak HRR almost twice as high as that of PIR without FRs but has a combustion time only half as long. Looking more closely at the THR curves at the end of combustion, the THR of PUR without FRs and PIR without FRs seem to be relatively similar. In summary, PUR without FRs shows an intense and fast combustion unlike the PIR system without FRs, which shows a weak but rather slow combustion. **Table 7** shows the comparison of data collected using MLC test and M-SBI test, such as the peak of heat release rate, THR, TSP.

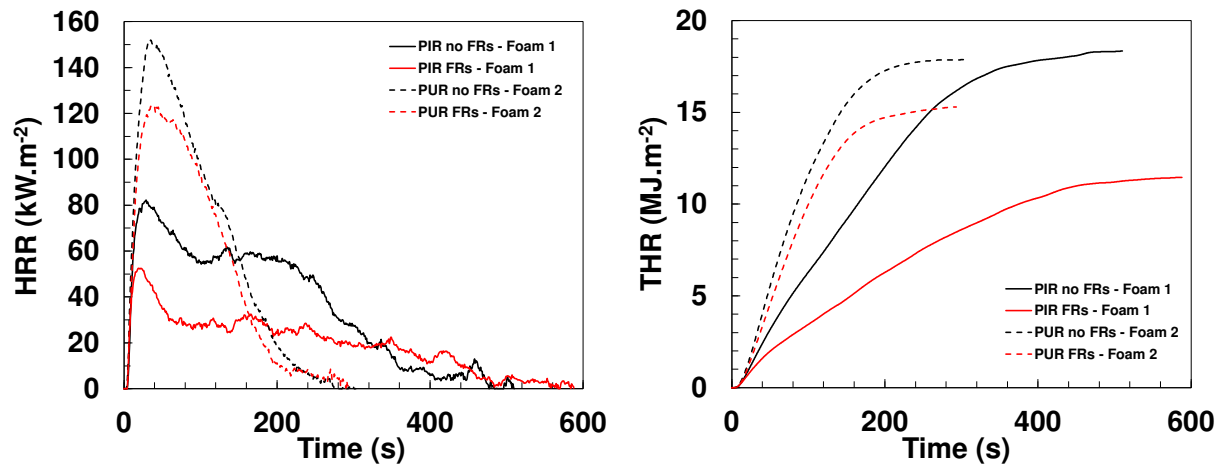


Figure 12: Heat release rate and total heat release of mass loss cone measurements under 35 kW.m^{-2} heat flux for PIR system and PUR system.

Table 7: Comparison between data collected using the MLC test (35 kW.m^{-2}) and M-SBI test ($1,51 \text{ kW}$).

Test	Parameter	PIR no FRs	PIR FRs	PUR no FRs	PUR FRs
MLC	Peak HRR (kW.m^{-2})	84	53	152	125
	THR (MJ.m^{-2})	18.1	11.4	17.8	15.2
	Total light attenuation (%)	1997	1311	4533	5313
M-SBI	Peak $\text{HRR}_{\text{av}(30 \text{ s})}$ (kW)	5.7	1.1	19.6	10.9
	$\text{THR}_{600\text{s}}$ (kJ)	385	261	2818	636
	$\text{TSP}_{600\text{s}}$ (m^2)	3.2	2.2	25.4	31.4

In the case of PIR foams with the MLC test, the use of FRs decreases the peak HRR (-37 %), THR (-37 %) and total light attenuation (-34 %). The same trend is observed with the use of M-SBI test with a decrease of peak $\text{HRR}_{\text{av}(30 \text{ s})}$ (-81 %), $\text{THR}_{600 \text{ s}}$ (-32 %) and $\text{TSP}_{600 \text{ s}}$ (-31 %). In the case of the M-SBI test, the peak $\text{HRR}_{\text{av}(30 \text{ s})}$ values exhibit a more pronounced difference than with the use of the MLC test. Indeed, with MLC test, the entire material is below the radiative flux, whereas in the case of M-SBI test, the spread of the flame over the material, either vertically or laterally, has a strong influence on the combustion and the peak HRR measured. As a reminder, **Figure 7** visually shows that the flame exceeds the PIR panel without FRs vertically, whereas the flame is only about halfway up in the PIR system with FRs.

In the case of PUR foams with the MLC test, the use of FRs decreases the peak HRR (-18 %) and THR (-15 %) while the total light attenuation increases (+17 %). This behavior has already been seen in literature. Indeed, different smoke behavior can be observed according to the FRs used [28–31]. The same trend is observed with M-SBI test but the difference between virgin and flame retarded foam is more pronounced. Indeed, during MLC tests, the entire foam is burned at once because the material is permanently exposed to the radiative flux contrary to the case of the M-SBI test, where there is a contribution of the flame spread effect to take into account. In the case of FR-PUR foam, no lateral propagation is observed as demonstrated by the measurement of the temperature profile. Therefore, only the part located above the burner burns. However, in the case of virgin PUR foam, the lateral propagation of the flame takes place and the two panels burn entirely. This is why the differences in the collected data between virgin and FR foam are more significant using the M-SBI test. The peak $\text{HRR}_{\text{av}(30 \text{ s})}$ decreases by 44 %, the $\text{THR}_{600\text{s}}$ by 77 % and the $\text{TSP}_{600 \text{ s}}$ increases by 24 %.

The trends observed in the M-SBI and MLC tests are almost identical in terms of heat and smoke release, which validate the M-SBI measurements. The use of the M-SBI allows to obtain a complementary approach to the MLC test thanks to a different fire scenario taking into account the lateral propagation of the flame. This test allows to discriminate the fire behavior of a material as does the MLC and to better understand the effect of flame retardants on foam.

4. Conclusions

The objective of this paper was to develop a small-scale SBI test and to demonstrate its efficiency considering the development of materials such as insulation foam used as case study. A new reduced scale bench test based on the standard SBI (EN138323) has been developed for research and development purposes and not for product certification. The experimental calibration protocol of the burner has been presented and validated. The addition of various equipment and sensors such as the use of a camera or thermocouples incorporated in the foam allowed a more accurate study of the combustion phenomenon.

PUR and PIR foams, which are widely used as insulation materials in construction applications were considered as case studies. The measurement of the various parameters (O_2 , CO_2 , T_{duct} , ΔP) allows determining crucial parameters such as FIGRA and SMOGRA. It was shown that the fire behavior of PIR and PUR systems differs. In the case of a polyisocyanurate foam, the addition of FRs leads to a decrease in the combustion intensity and the reduction of the smoke emitted. In the case of a polyurethane foam, the FRs allowed the reduction of the combustion intensity, the suppression of the flame spread, however, the smoke released increased.

The reduction of the size of the sample make it easier and cheaper the addition of sensors or other equipment to obtain additional data allowing to complete the understanding of the fire behavior of materials. To validate the heat and smoke release of the M-SBI, the obtained results were compared to MLC test results on the same materials. The M-SBI measurements correlate well with the MLC results and allow to discriminate the different formulations. The last step of the study is to correlate the M-SBI with the SBI, which is ongoing in our lab.

In order to go further, improvement of the M-SBI test could be considered. For example, the power of the burner, the size of the samples or the test time can be modified. It is also possible to imagine the addition of new sensors such as an infrared thermal camera to measure the surface temperature of the materials during burning, a scale under the frame to measure the mass loss during combustion or a gas analyzer placed in the exhaust duct to identify the gases evolved.

Acknowledgments

The authors want to thank BASF for supplying the foams and for funding the project.

References

- [1] L. Aditya, T.M.I. Mahlia, B. Rismanchi, H.M. Ng, M.H. Hasan, H.S.C. Metselaar, O. Muraza, H.B. Aditiya, A review on insulation materials for energy conservation in buildings, *Renewable and Sustainable Energy Reviews*. 73 (2017) 1352–1365. <https://doi.org/10.1016/j.rser.2017.02.034>.
- [2] H. Siddique, Grenfell Tower fire: police considering manslaughter charges, *The Guardian*. (2017). <https://www.theguardian.com/uk-news/2017/jun/23/grenfell-tower-fire-police-considering-manslaughter-charges> (accessed April 8, 2020).
- [3] M. McKee, Grenfell Tower fire: why we cannot ignore the political determinants of health, *British Medical Journal Publishing Group*, 2017.
- [4] A.F. Grand, C.A. Wilkie, *Fire retardancy of polymeric materials*, CRC Press, 2000.
- [5] J. Xin, C. Huang, Fire risk analysis of residential buildings based on scenario clusters and its application in fire risk management, *Fire Safety Journal*. 62 (2013) 72–78. <https://doi.org/10.1016/j.firesaf.2013.09.022>.
- [6] F.H. Prager, H. Rosteck, *Polyurethane and fire: fire performance testing under real conditions*, John Wiley & Sons, 2006.
- [7] J.M. Davies, *Lightweight Sandwich Construction*, John Wiley & Sons, 2008.
- [8] European Standard - Reaction to fire tests for building products - Building products excluding floorings exposed to the thermal attack by a single burning item. EN 13823:2002, (2002).
- [9] D. Drysdale, *An Introduction to Fire Dynamics*, John Wiley & Sons, 2011.
- [10] M. Poreh, G. Garrad, A study of wall and corner fire plumes, *Fire Safety Journal*. 34 (2000) 81–98.
- [11] W. Takahashi, O. Sugawa, H. Tanaka, M. Ohtake, Flame and Plume Behavior in and near a Corner of Walls, *Fire Safety Science*. 5 (1997) 261–271.
- [12] S. Bourbigot, P. Bachelet, F. Samyn, M. Jimenez, S. Duquesne, Intumescence as method for providing fire resistance to structural composites: application to poly(ethylene terephthalate) foam sandwich-structured composite, *Composite Interfaces*. 20 (2013) 269–277. <https://doi.org/10.1080/15685543.2013.793586>.
- [13] P. Tranchard, F. Samyn, S. Duquesne, M. Thomas, B. Estèbe, J.-L. Montès, S. Bourbigot, Fire behaviour of carbon fibre epoxy composite for aircraft: Novel test bench and experimental study, *Journal of Fire Sciences*. 33 (2015) 247–266.
- [14] A. De Corso, A. Castrovinci, Mini single burning item [miniSBI]: a unique lab-scale device to pre-screen reduced specimen for the EN 13823, *Fire Resistance in Plastics*. (2015) 8–10.
- [15] T. Hakkarainen, M.A. Kokkala, Application of a one-dimensional thermal flame spread model on predicting the rate of heat release in the SBI test, *Fire and Materials*. 25 (2001) 61–70. <https://doi.org/10.1002/fam.760>.
- [16] P. Van Hees, T. Hertzberg, A. Steen-Hansen, Development of a screening method for the SBI and room corner using the cone calorimeter, 2002.
- [17] ASTM E906 / E906M-17, Standard Test Method for Heat and Visible Smoke Release Rates for Materials and Products Using a Thermopile Method, ASTM International, West Conshohocken, PA, 2017, (2017).
- [18] ISO 5660-1:2015(en) Reaction-to-fire tests — Heat release, smoke production and mass loss rate — Part 1: Heat release rate (cone calorimeter method) and smoke production rate (dynamic measurement), (2015).
- [19] M.A. Dietenberger, C.R. Boardman, HRR upgrade to mass loss calorimeter and modified Schlyter test for FR Wood, in: *In: Proceedings of the Fire and Materials 2013 Conference Held at the Hyatt Hotel Fisherman’s Wharf Hotel, San Francisco, California, USA 28-30 January 2013*. Pp. 251-263., 2013: pp. 251–263.
- [20] A. Gharehbagh, Z. Ahmadi, Polyurethane Flexible Foam Fire Behavior, in: F. Zafar (Ed.), *Polyurethane*, InTech, 2012. <https://doi.org/10.5772/47965>.
- [21] X. Liu, J. Hao, S. Gaan, Recent studies on the decomposition and strategies of smoke and toxicity suppression for polyurethane based materials, *RSC Advances*. 6 (2016) 74742–74756. <https://doi.org/10.1039/C6RA14345H>.

- [22] J. Troitzsch, *International plastics flammability handbook : principles-regulations-testing and approval*, 1983.
- [23] S.A. Omer, S.B. Riffat, G. Qiu, Technical note: Thermal insulations for hot water cylinders: a review and a conceptual evaluation, *Building Services Engineering Research and Technology*. 28 (2007) 275–293. <https://doi.org/10.1177/0143624406075269>.
- [24] S. Gaan, S. Liang, H. Mispreve, H. Perler, R. Naescher, M. Neisius, Flame retardant flexible polyurethane foams from novel DOPO-phosphonamidate additives, *Polymer Degradation and Stability*. 113 (2015) 180–188. <https://doi.org/10.1016/j.polymdegradstab.2015.01.007>.
- [25] A. Granzow, Flame retardation by phosphorus compounds, *Acc. Chem. Res.* 11 (1978) 177–183. <https://doi.org/10.1021/ar50125a001>.
- [26] M. Checchin, C. Cecchini, B. Cellarosi, F.O. Sam, Use of cone calorimeter for evaluating fire performances of polyurethane foams, *Polymer Degradation and Stability*. 64 (1999) 573–576. [https://doi.org/10.1016/S0141-3910\(98\)00131-1](https://doi.org/10.1016/S0141-3910(98)00131-1).
- [27] B. Youssef, B. Mortaigne, M. Soulard, J.M. Saiter, Fireproofing of polyurethane by organophosphonates: Study of degradation by simultaneously TG/DSC, *J Therm Anal Calorim.* 90 (2007) 489–494. <https://doi.org/10.1007/s10973-006-7971-x>.
- [28] Y. Chung, Y. Kim, S. Kim, Flame retardant properties of polyurethane produced by the addition of phosphorous containing polyurethane oligomers (II), *Journal of Industrial and Engineering Chemistry*. 15 (2009) 888–893. <https://doi.org/10.1016/j.jiec.2009.09.018>.
- [29] D. Xu, K. Yu, K. Qian, Effect of tris(1-chloro-2-propyl)phosphate and modified aramid fiber on cellular structure, thermal stability and flammability of rigid polyurethane foams, *Polymer Degradation and Stability*. 144 (2017) 207–220. <https://doi.org/10.1016/j.polymdegradstab.2017.08.019>.
- [30] M. Zhang, J. Zhang, S. Chen, Y. Zhou, Synthesis and fire properties of rigid polyurethane foams made from a polyol derived from melamine and cardanol, *Polymer Degradation and Stability*. 110 (2014) 27–34. <https://doi.org/10.1016/j.polymdegradstab.2014.08.009>.
- [31] W. Xu, G. Wang, Influence of thermal behavior of phosphorus compounds on their flame retardant effect in PU rigid foam: Influence of phosphorus compounds on PU rigid foam, *Fire Mater.* 40 (2016) 826–835. <https://doi.org/10.1002/fam.2346>.